Chapter 4

Physical processes causing asymmetry of tide-dominated ebb-tidal deltas

Abstract

In Chapter 3 an idealized model was developed to study physical processes that maintain the spatially symmetric ebb-tidal delta. In this chapter the idealized model of Chapter 3 is extended with physical processes that lead to asymmetric ebb-tidal deltas. The focus is on tide-dominated systems. The following tide-related processes are added: Coriolis force, large-scale shore-parallel tidal currents and large-scale shore-parallel residual currents. Including the Coriolis force results in a small asymmetry of the ebb-tidal delta. For the Northern Hemisphere the model predicts that the area with ebb-dominated currents is located at the right-hand side of the tidal inlet (when viewing from the inlet in the seaward direction). The ebb-tidal delta is located at the seaward end of the area with ebb-dominated currents. No ebb-dominated channel is modeled. The delta is called right-oriented. On the left-hand side of the mid-axis of the inlet a channel is modeled, which has flood-dominated currents. Shore-parallel tidal currents have a strong influence on the asymmetry of ebb-tidal deltas. For a parameter setting that is representative for the Dutch Wadden coast, the area with ebb-dominated currents is located at the left-hand side of the mid-axis of the inlet. An increase of the phase difference between shore-parallel and cross-shore tidal currents results in a less asymmetric delta and ultimately its orientation changes. Increasing the magnitude of the shore-parallel currents while keeping the cross-shore tidal currents constant, leads to an increase of the asymmetry of the deltas. The influence of the residual shore-parallel currents on the characteristics of the deltas is also large. A residual current from left to right (when viewing in seaward direction) leads to a right-oriented delta. A residual current from right to left leads to a left-oriented delta. Model results are compared with observations of the ebb-tidal deltas of the tidal inlet systems of the Dutch Wadden Sea. The modeled current patterns agree well with observed ones. The modeled bottom patterns are consistent with the bottom patterns as found in Chapters 3 and 5. Furthermore, the position of the ebb-tidal delta corresponds with observed ones. However, the model is not able to reproduce the observed ebb-dominated channel.

4.1 Introduction

Ebb-tidal deltas are shallow sandy structures situated at the seaward side of tidal inlets. They are observed in many parts of the world (*Ehlers*, 1988; *Sha*, 1989a; *FitzGerald*, 1996; *Davis*, 1997; *Hicks et al.*, 1999). The center of the deltas are located at the seaward end of an area with ebb-dominated currents (i.e., stronger peak currents during the ebb-phase than during the flood-phase). The delta folds around the ebb-dominated channel. Close to the coast two flood-dominated channels are found (*Hayes*, 1975). Necessary conditions for the emergence of ebb-tidal deltas are a sandy bottom and the presence of strong tidal currents. Apart from tidal currents, waves are often an important constituent of the water motion in the region of the ebb-tidal delta (*Sha*, 1989a; *FitzGerald*, 1996). Since the strength of the tidal currents and wave influence varies orders of magnitude for the ebb-tidal deltas around the world, *Gibeaut and Davis Jr.* (1993) identified three major classes of deltas, i.e., tide-dominated, mixed-energy and wave-dominated deltas. These different classes of deltas have different characteristics. This makes it inevitable to limit the scope of this study. Here, only tide-dominated deltas are studied.

In Chapter 3 the tide-dominated ebb-tidal deltas along the eastern US-coast (Georgia, South Carolina) were discussed. It was noticed that they are almost symmetric with respect to reflections about the mid-axis through the center of the inlet. The ebb-dominated channels have a shore-normal orientation. The shore-parallel currents along the east US-coast are small compared to the cross-shore tidal currents through the inlets. A barrier coast where shore-parallel currents have the same order of magnitude as the cross-shore tidal currents is found along the Dutch and German Wadden coast. Also in this area tide-dominated ebb-tidal deltas are found, but they are not spatially symmetric (*Ehlers*, 1988; *Sha*, 1989a; *FitzGerald*, 1996). Here, we introduce the convention that left-hand (right-hand) side is always defined as left (right) when viewing from the inlet in the seaward direction. If the ebb-dominated channel is oriented to the left the ebb-tidal delta is called left-oriented. When the area with ebb-dominated currents is found on the right-hand side the delta is called right-oriented. In Figure 4.1(a) the channels and deltas along the Dutch Wadden Sea are shown. The black contour line represents the outlines of the ebb-tidal deltas. The dark shaded parts represent the channels. Most of them are ebb-dominated and are oriented to the left. In addition, also most sediment of the delta seems to be located at the left-hand side of mid-axis of the inlet. In Figure 4.1(b) the deltas and ebb-dominated channels along the German Wadden Sea are shown. The position of the ebb-tidal deltas is represented by the black contour line and the position of the channels by the dark shaded parts. In this area most ebb-dominated channels are right-oriented.

The observed variation in the orientation of the ebb-dominated channels raises the question which physical process can lead to the oblique orientation of the ebb-dominated channel. In the conceptual model of *Sha* (1989a,b) it is argued that the asymmetry is caused by the interaction between the shore-parallel and cross-shore tidal currents. This interaction causes weaker and more rotary currents at the right-hand side of the tidal inlet. On the left-hand side the tidal currents are stronger and sediment is eroded from the bed. Hence, the ebb-dominated channel is oriented to the left (see Figure 4.2). Furthermore, most sand of the ebb-tidal delta is found on the left-hand side. In contrast, obliquely

incident waves can cause the ebb-dominated channel to be oriented to the right (see *Oertel* (1975); *FitzGerald* (1996) and references therein). Obliquely incident waves refract and break in the surf zone and this results in a wave-driven current. Assume that far away from the tidal inlet the wave-drive currents are from left to right and transport sediment. The presence of the tidal inlet causes an interruption of the wave-driven currents, because the waves do not break in the inlet where the depths are large. This interruption causes deposition at the left-hand side of the tidal inlet and erosion of sediment at the right-hand side. Hence, the main channel will be right-oriented. This effect becomes more important when wave influence becomes more important.

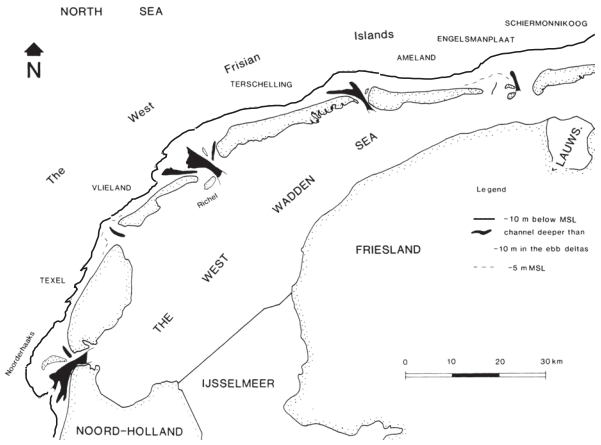

(a)

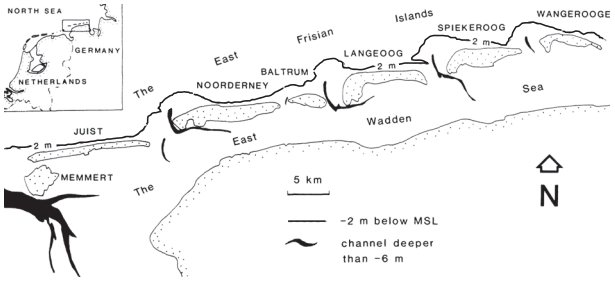

(b)

Figure 4.1: (a) Channels and deltas along the Dutch Wadden Sea. Dark contour line represents the 10 meter depth contour line and shows the presence of the ebb-tidal deltas. The dark shaded parts represent the channels with more than 10 meter depth. (b) Channels and shoals along the German Wadden Sea. The 2 meter depth contour line shows the presence of the ebb-tidal deltas. Dark shaded parts are channels with more than 6 meter depth. Both figures after *Sha* (1989a).

Process-based models are needed to validate the conceptual models of *Oertel* (1975); *Sha* (1989a); *FitzGerald* (1996). State-of-the-art process-based models have been used to study the initial response (*van Leeuwen and de Swart*, 2002; *Schuttelaars et al.*, 2003;

Siegle et al., 2004) and the long-term evolution (*Cayocca*, 2001; *van Leeuwen et al.*, 2003) of asymmetric ebb-tidal deltas under various forcing conditions. In view of the aim of the present study, the results of *van Leeuwen et al.* (2003) are of specific interest. They simulated the temporal evolution of the bathymetry of the Frisian Inlet (located between the islands of Ameland and Schiermonnikoog, see Figure 4.1(a)), starting from a state without a delta and with a backbarrier basin having a constant depth of 2 m. During the simulation an asymmetric ebb-tidal delta developed and after a long time ($\sim$ 500 years) the bathymetric changes decreased. Due to numerical resolution problems a true morphodynamic equilibrium was not reached. In addition, their results suggest that the mechanism proposed by *Sha* (1989a) can not completely explain the asymmetric shape of ebb-tidal deltas. They found that the currents on the left-hand side of the inlet are indeed bidirectional and ebb-dominated as argued by *Sha* (1989b), but this did not result in a preferred erosion of sediment.

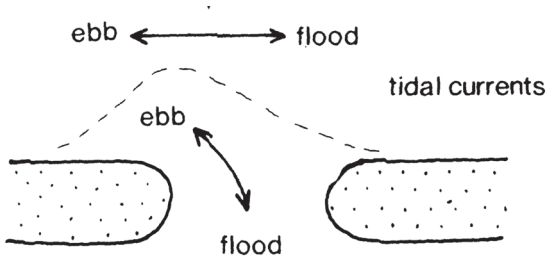

Figure 4.2: Sketch presented by *Sha* (1989a) to explain the asymmetry of tide-dominated deltas along the Dutch Wadden Sea. Due to interaction of shore-parallel tidal currents and cross-shore tidal currents are maximum ebb-currents oriented to the left of the inlet.

The results of *van Leeuwen et al.* (2003) motivated *van der Vegt et al.* (2005) to develop and analyze an idealized morphodynamic model to answer the question whether ebb-tidal deltas can be modeled as morphodynamic equilibria. Rather than calculating the temporal evolution of a tidal inlet system, they developed a direct method to calculate the equilibrium solutions (characterized by a steady bottom pattern) of such a system. They found morphodynamic equilibria that resemble observed ebb-tidal deltas. The focus of their study was on symmetric deltas such as those found along the US-coast. Therefore, they ignored the Coriolis force, prescribed a symmetric velocity profile over the inlet, did not allow for large-scale alongshore pressure gradients related to propagation of the tide along the coast, did not allow for large-scale alongshore residual currents and only accounted for shore-normal incident waves.

A fundamental process-based understanding of the processes that cause asymmetry of tide-dominated deltas is still missing. Therefore the main aim of this study is to investigate the physical processes related to tides which cause such deltas to be asymmetric. This is done by extending the model of *van der Vegt et al.* (2005) with processes that can lead to asymmetry. The influence of the following processes on the (a)symmetry of ebb-tidal deltas are studied:

- Coriolis force;
- Large scale alongshore pressure gradients at sea;
- Residual alongshore currents at sea;

This study proceeds as follows. In Section 4.2 the model is described, followed by an analysis of the equations of motion in Section 4.3. In Section 4.4 the method to calculate morphodynamic equilibrium solutions is shortly explained. A detailed explanation can be found in *van der Vegt et al.* (2005). Then the three agents causing asymmetry of the ebb-tidal delta are studied in Section 4.5. Section 4.6 contains a discussion and ends with suggestions for further research.

4.2 Model description

4.2.1 Domain

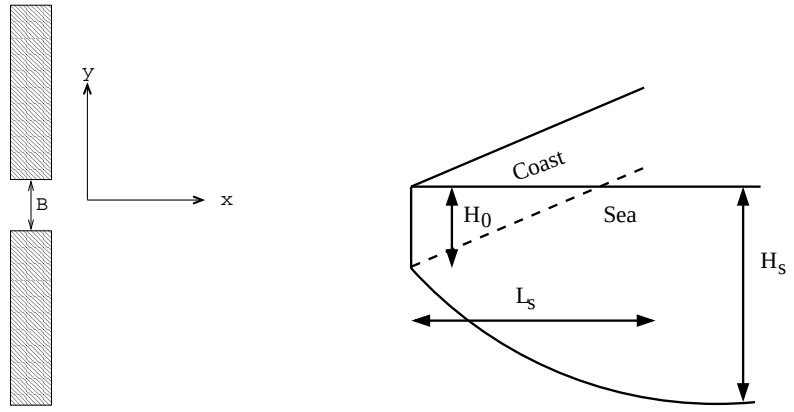

Figure 4.3: (a) Inlet of width B is centered around $(x, y) = (-x_s, 0)$. (b) Side view of model. For more information see text.

The model domain consists of a coastal sea that is bounded by a straight coast. The latter is interrupted by one inlet (having a width B). A Cartesian coordinate system is used, with the x, y, z-axes pointing in the cross-shore, alongshore and upward direction, respectively. The coastline is located at $x = -x_s$, while the center of the interruption of the coast is at $(x, y) = (-x_s, 0)$, as is sketched in Figure 4.3(a). The transition from the nearshore zone to the inner shelf is located at $x = 0$. In the nearshore zone the dynamics is mainly determined by complex wave-driven processes. At the inner shelf the tide is the dominant constituent of the water motion. It is assumed that there is no interaction between the nearshore zone and the inner shelf. The domain on which the calculations are performed is $x \in [0, \infty)$ and $y \in (-\infty, +\infty)$.

The position of the bottom is denoted by $z = -H$, with H the undisturbed water depth. In the regions far away from the inlet the bathymetry is given by $H = H_{\mathrm{R}}(x)$, where

$$H_{\mathrm{R}}(x) = H_0 + (H_s - H_0)(1 - e^{-x/L_s}) \tag{4.1}$$

Here, H_0 is the undisturbed water depth at $x = 0$. This water depth increases exponentially to a value $H_s > H_0$ in the cross-shore direction (Figure 4.3(b)). Typical values for

the Dutch coast are $H_0 = 5$ m, $H_s = 25$ m and an e-folding length scale $L_s = 10$ km (see Chapter 2).

4.2.2 Currents

The hydrodynamics is described by the depth-averaged shallow water equations. A semi-diurnal lunar (M_2) tide is considered (frequency $\sigma \sim 1.4 \times 10^{-4}$ s^{-1}) and the tidal wave has a characteristic wavelength $L_g = 2\pi\sqrt{gH}/\sigma \sim$ 300 km in water with a depth of 5 meter. It is assumed that the spatial scales of interest (spatial scale of the ebb-tidal delta, width of the tidal inlet) are small compared to the wavelength of the tidal wave. This allows for a rigid lid approximation: The sea level variations itself are not important, but the spatial gradients result in pressure gradients in the momentum equations (see e.g., *Huthnance* (1982); *Calvete et al.* (2001)). The hydrodynamic equations become

$$\frac{\partial u}{\partial t} + u\frac{\partial u}{\partial x} + v\frac{\partial u}{\partial y} - fv = -g\frac{\partial \zeta}{\partial x} - \frac{\tau_x}{\rho H} + A_h\Big(\frac{\partial^2 u}{\partial x^2} + \frac{\partial^2 u}{\partial y^2}\Big) \tag{4.2a}$$

$$\frac{\partial v}{\partial t} + u\frac{\partial v}{\partial x} + v\frac{\partial v}{\partial y} + fu = -g\frac{\partial \zeta}{\partial y} - \frac{\tau_y}{\rho H} + A_h\Big(\frac{\partial^2 v}{\partial x^2} + \frac{\partial^2 v}{\partial y^2}\Big) \tag{4.2b}$$

$$\frac{\partial (uH)}{\partial x} + \frac{\partial (vH)}{\partial y} = 0 \tag{4.2c}$$

Here, u is the cross-shore component and v the alongshore component of the velocity vector $\vec{u}$, t is time, f is the Coriolis parameter, H the water depth, ζ the surface elevation, τ_x, τ_y are the cross-shore and alongshore component of the bed shear-stress vector $\vec{\tau}$, g the acceleration due to gravity, ρ the density of water and A_h the horizontal eddy viscosity coefficient. The latter depends on the amplitude of the tidal currents and is modeled as $A_h = lU$, with $l \sim 10$ m a mixing length scale and $U \sim 1$ ms^{-1} a characteristic velocity scale related to the strength of the tidal currents. This U will be defined in Section 4.3.2. This formulation accounts for both mixing by small-scale turbulent eddies and vertical shear dispersion (*Zimmerman*, 1986).

A formulation for the bed shear-stress is used that is linear in the current

$$\vec{\tau} = \rho r \vec{u} \tag{4.3}$$

In this study a spatially uniform friction coefficient r is chosen, which is defined as

$$r = \frac{8}{3\pi} C_d U \tag{4.4}$$

Here, $C_d (\sim 0.0025)$ is a drag coefficient and U is a characteristic flow amplitude of the domain and is related to the intensity of the tidal currents. The water motion in the domain is forced by prescribed cross-shore tidal currents in the inlet and by large-scale alongshore pressure gradients induced by the tidal wave. The boundary conditions are that the tidal currents in the inlet are prescribed. Far away from the inlet the tidal currents have their magnitude due to the prescribed large-scale alongshore pressure gradient.

4.2.3 Sediment transport

It is assumed that the sediment is relatively coarse and that its transport takes place as bedload (see *van Leeuwen et al.* (2003) and *van der Vegt et al.* (2005)). A Bagnold-Bailard sediment transport formulation is used, which is based on concepts discussed by *Bagnold* (1966) and *Bailard* (1981). This formulation requires information of the currents at about 5 cm from the bed. Therefore, the depth-averaged currents (denoted by $\vec{u}$, having component u and v) have to be transformed to the magnitude of the currents at that specific position ($\vec{u}_{bl}$). This is done by assuming a logarithmic profile of the horizontal current and choosing a specific roughness height (here, the grain size of $\sim$0.3 mm). Thus, Coriolis effects (causing veering of the currents over the vertical) are neglected. This yields $\vec{u}_{bl} = \beta\vec{u}$, with $\beta \approx 0.35$ a constant factor. Note that in the model of Chapter 3 it was implicitly assumed that $\beta = 1$.

The sediment transport is split into two different contributions. The first is the sediment transport induced by the tidal currents and the second is the sediment transport induced by the presence of the bed-slopes. The bedload transport averaged over the tidal period reads

$$\vec{q} = \vec{q}_{\rm f} + \vec{q}_{\rm bot} \tag{4.5}$$

with

$$\vec{q}_{\rm f} = \alpha\beta^3 < |\vec{u}|^2\vec{u} > \tag{4.6}$$

$$\vec{q}_{\rm bot} = \alpha\gamma\beta^p U^p \vec{\nabla}\tilde{H} \tag{4.7}$$

Here, the brackets $< . >$ denote an averaging over the tidal period. The constant α depends on sediment characteristics and has for a grain size of $\sim$ 0.3 mm a value of $\alpha = 10^{-5}$ s^{2}m^{-1}. The bed-slope coefficient γ is ~ 1 $(\frac{m}{s})^{3-p}$ with p a constant. It has been argued that its value should be ~ 2, *Struiksma et al.* (1985), or ~ 3 in *Bailard* (1981) and *Sekine and Parker* (1992). Here, a value of $p = 2$ will be used. Furthermore, U is the characteristic velocity scale which will be defined in Section 4.3.2. The variable $\tilde{H}$ in Equation (4.7) is the deviation of the bathymetry from the reference bathymetry, $\tilde{H} = H - H_{\rm R}$. Note that Equation (4.7) implies that only deviations of the reference bathymetry cause bed-slope induced sediment transport. This is allowed since the spatial scales of the ebb-tidal delta (the width B) are much smaller than the typical scale of the reference bathymetry (the e-folding length scale L_s) and therefore the typical magnitude of $\vec{\nabla}H_{\rm R}$ is much smaller that of $\vec{\nabla}\tilde{H}$.

4.2.4 Sediment mass conservation and morphodynamic equilibrium

When the sediment transport is convergent the water depth will decrease because the sediment is deposited at the bed. In case of a divergent sediment transport the total water depth will increase. Furthermore, the time scale on which bottom patterns evolve is much larger than the time scale of the hydrodynamics (period of the M_2 tide). This allows for calculating the hydrodynamics with a constant bathymetry while the evolution of the bed

is driven by the convergence of the residual sediment transport (for mathematical details about this tidal averaging method see *Sanders and Verhulst* (1985)). The bed evolution equation reads

$$\frac{\partial H}{\partial t} - \vec{\nabla} \cdot \vec{q} = 0 \tag{4.8}$$

The aim of this study is to calculate morphodynamic equilibrium solutions of the model. They obey the condition

$$\frac{\partial H}{\partial t} = 0 \tag{4.9}$$

which implies, according to Equation (4.8), that the sediment flux should have zero divergence. Henceforth we assume that $H(x, y)$ represents an equilibrium. The boundary conditions are that far away from the inlet the bathymetry is given by the reference bathymetry, as given in Equation (4.1). In the tidal inlet a regularity conditions is applied which states that the depth is finite. Outside the inlet it is required that the cross-component of $\vec{q}$ vanishes.

4.3 Reference state and inlet state

The model allows for a morphodynamic equilibrium which is alongshore uniform. This so-called reference state is obtained by considering the case without tidal currents through the tidal inlet. The water motion is only forced by the large-scale pressure gradient. In case an inlet is present this reference state is obviously modified. Hence, the state variables are split into a part which is due to the prescribed large-scale pressure gradient and a part which is due to the prescribed cross-shore tidal currents through the tidal inlet (denoted by a tilde):

$$\begin{aligned} \vec{u} &= \vec{U} + \vec{\tilde{u}}; \qquad u = U + \tilde{u}; \qquad v = V + \tilde{v}; \qquad \vec{\nabla}\zeta = \vec{\nabla}Z + \vec{\nabla}\tilde{\zeta}; \\ \vec{q} &= \vec{Q} + \vec{\tilde{q}}; \qquad \vec{q}_{\mathrm{f}} = \vec{Q}_{\mathrm{f}} + \vec{\tilde{q}}_{\mathrm{f}}; \qquad \vec{q}_{\mathrm{bot}} = \vec{Q}_{\mathrm{bot}} + \vec{\tilde{q}}_{\mathrm{bot}}; \qquad H = H_{\mathrm{R}} + \tilde{H} \end{aligned} \tag{4.10}$$

In the next section the reference state morphodynamic equilibrium is described. This section is followed by a section in which the morphodynamic equilibrium due to the presence of the tidal inlet is described.

4.3.1 Reference state morphodynamic equilibrium

Hydrodynamics

In the present model the gradient of Z is spatially uniform and it forces shore-parallel currents which are alongshore uniform. In the reference state the cross-shore velocity is zero ($U = 0$) and the bathymetry is taken alongshore uniform. Substituting Equation (4.10) into Equations (4.2a)-(4.2c) and assuming that all variables due to the presence of the tidal inlet are zero leads to the equations that describe the hydrodynamics of the reference

state. The momentum balance in the alongshore direction comprises a balance between local inertia, the pressure gradient due to the alongshore sea surface gradient, friction and diffusive terms. However, diffusive terms are only important in the nearshore zone $x \in (-x_s, 0)$ due to the boundary condition at $x = -x_s$. The boundary layer thickness ($\sim \sqrt{A_h/\sigma}$) is small compared to the width of the nearshore zone (x_s). In the region $x > 0$ a scaling analysis reveals that the diffusive terms are small compared to the other terms in the reference state alongshore momentum equation. Because we are only interested in the region outside the nearshore zone, it can be used that $A_h \frac{\partial^2 V}{\partial x^2}$ is small compared to the other terms in the alongshore momentum balance. Consequently, Equations (4.2a) and (4.2b) for the reference state become

$$fV = g\frac{\partial Z}{\partial x} \tag{4.11a}$$

$$\frac{\partial V}{\partial t} = -g\frac{\partial Z}{\partial y} - \frac{rV}{H_{\mathrm{R}}} \tag{4.11b}$$

Note that Equation (4.11a) describes geostrophic balance. Following the description of the basic state in Chapter 2, the large-scale alongshore pressure gradient due to the tidal wave is written as

$$-g\frac{\partial Z}{\partial y} = S_0 + S_2 \cos(\sigma t + \phi_a) \tag{4.12}$$

with S_0 a residual component and S_2 the magnitude of the tidal (M_2) component. Furthermore, ϕ_a is an arbitrary phase to control the phase difference between the prescribed currents in the tidal inlet and the alongshore tidal currents at sea induced by the large-scale pressure gradient. The solution of Equation (4.11b) can be found in *Calvete et al.* (2001) and reads

$$V(x) = V_0(x) + V_2(x)\cos(\sigma t - \Phi(x)) \tag{4.13}$$

where

$$V_0 = \frac{S_0 H_{\mathrm{R}}}{r}; \qquad V_2(x) = \frac{H_{\mathrm{R}}(x) S_2}{\sqrt{H_{\mathrm{R}}(x)^2 + (r/\sigma)^2}}; \qquad \Phi(x) = \arctan\left(\frac{r}{\sigma H_{\mathrm{R}}(x)}\right) + \phi_a \tag{4.14}$$

Net sediment transport

The net sediment transport in the reference state is obtained by substituting Equation (4.10) into Equations (4.6)- (4.7). This yields

$$\vec{Q}_{\mathrm{f}} = \alpha\beta^3 < |\vec{U}|^2 \vec{U} > \tag{4.15}$$

$$\vec{Q}_{\mathrm{bot}} = 0 \tag{4.16}$$

Note that $\vec{Q}_{\mathrm{f}}$ is only nonzero when V_0 is nonzero. In that case $\vec{Q}_{\mathrm{f}}$ only has an alongshore component, which is alongshore uniform.

Morphodynamic equilibrium

In the reference state the sediment mass balance becomes

$$\vec{\nabla} \cdot \vec{Q}_{\mathrm{f}} = 0 \tag{4.17}$$

Note that $\vec{\nabla} \cdot \vec{Q}_{\mathrm{f}} = 0$, because $\vec{Q}_{\mathrm{f}}$ is alongshore uniform.

4.3.2 Morphodynamic equilibrium due to presence of tidal inlet

Hydrodynamics

The equations that describe the hydrodynamics due to the presence of a tidal inlet are obtained by substituting Equation (4.10) into Equations (4.2a)-(4.2c), subtracting Equations (4.11a)-(4.11b) that describe the reference state and finally using that $A_h \frac{\partial^2 V}{\partial x^2} = 0$. The results are

$$\frac{\partial \tilde{u}}{\partial t} + \tilde{u}\frac{\partial \tilde{u}}{\partial x} + (V+\tilde{v})\frac{\partial \tilde{u}}{\partial y} - f\tilde{v} = -g\frac{\partial \tilde{\zeta}}{\partial x} - \frac{r\tilde{u}}{H_{\mathrm{R}}+\tilde{H}} + A_h\big(\frac{\partial^2 \tilde{u}}{\partial x^2} + \frac{\partial^2 \tilde{u}}{\partial y^2}\big) \tag{4.18a}$$

$$\frac{\partial \tilde{v}}{\partial t} + \tilde{u}\frac{\partial (V+\tilde{v})}{\partial x} + (V+\tilde{v})\frac{\partial (V+\tilde{v})}{\partial y} + f\tilde{u} = -g\frac{\partial \tilde{\zeta}}{\partial y} - \frac{r(V+\tilde{v})}{H_{\mathrm{R}}+\tilde{H}} + \frac{rV}{H_{\mathrm{R}}} + A_h\big(\frac{\partial^2 \tilde{v}}{\partial x^2} + \frac{\partial^2 \tilde{v}}{\partial y^2}\big) \tag{4.18b}$$

$$\frac{\partial}{\partial x}[\tilde{u}(H_{\mathrm{R}}+\tilde{H})] + \frac{\partial}{\partial y}[(V+\tilde{v})(H_{\mathrm{R}}+\tilde{H})] = 0 \tag{4.18c}$$

The rigid lid approximation allows for a convenient way to solve the hydrodynamic equations by constructing an equation for the vorticity. The vorticity is defined as $\omega = \partial v/\partial x - \partial u/\partial y$. Following the splitting of the variables as in Equation (4.10), we define $\omega = \Omega + \tilde{\omega}$ with $\Omega = \partial V/\partial x$ and $\tilde{\omega} = \partial \tilde{v}/\partial x - \partial \tilde{u}/\partial y$. Taking the derivative of Equation (4.18b) with respect to x and subtracting the derivative of Equation (4.18a) with respect to y results in an equation for the vorticity,

$$\begin{aligned}\frac{\partial \tilde{\omega}}{\partial t} + \tilde{u}\frac{\partial (\Omega+\tilde{\omega})}{\partial x} + (V+\tilde{v})\frac{\partial \tilde{\omega}}{\partial y} &= -(\Omega+\tilde{\omega}+f)\big(\frac{\partial \tilde{u}}{\partial x} + \frac{\partial \tilde{v}}{\partial y}\big) - \frac{r(H_{\mathrm{R}}\tilde{\omega} - \tilde{H}\Omega)}{H_{\mathrm{R}}(H_{\mathrm{R}}+\tilde{H})} \\ &\quad + \frac{r}{(H_{\mathrm{R}}+\tilde{H})^2}\big[(V+\tilde{v})\frac{\partial (H_{\mathrm{R}}+\tilde{H})}{\partial x} - \tilde{u}\frac{\partial \tilde{H}}{\partial y}\big] \\ &\quad - \frac{rV}{H_{\mathrm{R}}^2}\frac{dH_{\mathrm{R}}}{dx} + A_h\big(\frac{\partial^2 \tilde{\omega}}{\partial x^2} + \frac{\partial^2 \tilde{\omega}}{\partial y^2}\big)\end{aligned} \tag{4.19}$$

The vorticity equation (4.19) and the continuity equation (4.18c) are solved in the model with boundary conditions

$$x = 0, \quad |y| > B/2 : \qquad \tilde{u} = 0, \frac{\partial \tilde{v}}{\partial x} = 0 \tag{4.20a}$$

$$x = 0, \quad |y| < B/2 : \qquad \tilde{u} = \hat{U}(y)\cos(\sigma t), \frac{\partial \tilde{v}}{\partial x} = 0 \tag{4.20b}$$

$$(x^2 + y^2) \rightarrow \infty : \qquad \tilde{u} \rightarrow 0, \tilde{v} \rightarrow 0 \tag{4.20c}$$

At $x = 0$ a free-slip condition for the alongshore velocity component is applied. Furthermore, $\hat{U}(y)$ is a given cross-shore tidal current profile in the inlet,

$$\hat{U}(y) = \hat{U}(0)\big[(2\frac{y}{B} - 1)^3(2\frac{y}{B} + 1)^3\big] \tag{4.21}$$

where $\hat{U}(0)$ is the maximum current amplitude in the center of the inlet. This models an oscillating vorticity dipole in the inlet. The profile has been chosen such that both velocity and vorticity vanish at the boundaries $y = \pm B/2$. This is consistent with observations, which show that the velocity in the center of the tidal inlet is larger than at both sides of the tidal inlet (*Chadwick and Largier*, 1999). This velocity profile was also used in Chapter 3 of this thesis.

The typical scale of the velocity through the inlet and the typical scale of the shore-parallel tidal currents are known. From these two velocity scales the typical velocity scale of the domain (U) is determined. It is chosen as

$$U = \sqrt{\hat{U}(0)^2 + V_2(0)^2} \tag{4.22}$$

Sediment transport

The sediment transport due to the prescribed cross-shore tidal currents over the inlet is obtained by subtracting the reference state sediment transport from equations (4.6)-(4.7)

$$\vec{\tilde{q}}_{\mathrm{f}} = \alpha\beta^3(< |(\vec{U} + \vec{\tilde{u}})|^2(\vec{U} + \vec{\tilde{u}} > - < |\vec{U}|^2\vec{U} >) \tag{4.23}$$

$$\vec{\tilde{q}}_{\mathrm{bot}} = \alpha\gamma\beta^2U^2\vec{\nabla}\tilde{H} \tag{4.24}$$

Morphodynamic equilibrium

The sediment mass balance in morphodynamic equilibrium due to the presence of the tidal inlet is obtained by substituting Equations (4.23) and (4.24) into the morphodynamic equilibrium condition ($\vec{\nabla} \cdot \vec{q} = 0$) and subtracting the reference state equilibrium condition (4.15)- (4.17). The result is

$$\vec{\nabla} \cdot \vec{\tilde{q}}_{\mathrm{f}} + \vec{\nabla} \cdot \vec{\tilde{q}}_{\mathrm{bot}} = \vec{\nabla} \cdot \vec{\tilde{q}}_{\mathrm{f}} + \alpha\gamma\beta^2U^2\nabla^2\tilde{H} = 0 \tag{4.25}$$

The boundary conditions are

$$x = 0, |y| > \frac{B}{2} : \qquad \partial\tilde{H}/\partial x = 0 \tag{4.26a}$$

$$x = 0, |y| < \frac{B}{2} : \qquad \tilde{H} = \text{finite} \tag{4.26b}$$

$$(x^2 + y^2) \to \infty : \qquad \tilde{H} \to 0 \tag{4.26c}$$

Outside the inlet at $x = 0$ no exchange of sediment between the nearshore zone and the inner shelf is allowed. This implies that the cross-shore component of $\vec{\tilde{q}}$ is zero. From Equation (4.23) it follows that the cross-shore component of $\vec{\tilde{q}}_{\text{f}}$ is zero and therefore outside the inlet at $x = 0$ it is required that $\partial\tilde{H}/\partial x = 0$. In the inlet a regularity condition for the water depth is required. Far from the inlet the bathymetry tends to the reference bathymetry $H_R(x)$.

4.4 Methods

4.4.1 Finding morphodynamic equilibria

Morphodynamic equilibria in the model are obtained as follows. The starting point is a known equilibrium of the model (e.g., the reference equilibrium). The corresponding bathymetry is denoted by $H = H(x, y; \mu)$, where μ represents a parameter (e.g., $\hat{U}(0)$). Next, the value of μ is changed by a small increment $\Delta\mu$ and the tidal currents are computed using the 'old' bathymetry $H = H(x, y; \mu)$. From this, the sediment flux vector $\vec{\tilde{q}}_{\text{f}}$ is calculated from Equation (4.23) and next Equation (4.25) is solved to obtain a first guess for the 'new' equilibrium bottom $H = H(x, y; \mu + \Delta\mu)$. This boils down to finding the solution of a Poisson equation. This is not yet the 'true' bottom, because $\vec{\tilde{q}}_{\text{f}}$ was computed with a previous guess of the bottom pattern. So, an iteration procedure is applied which involves recomputation of the tidal currents with the new guess of the bottom and finding subsequent updates for $\vec{\tilde{q}}_{\text{f}}$ and $H = H(x, y; \mu + \Delta\mu)$ until convergence is established. After this, parameter μ can be changed again, resulting in a continuum of equilibrium solutions obtained for different parameter values. The success of this method was already demonstrated in Chapter 3.

4.4.2 Method to solve hydrodynamic equations

To numerically solve Equations (4.18c), (4.19) with boundary conditions (4.20), a pseudospectral method is used in the spatial coordinates (*Boyd*, 2001). For the time-dependent part a Galerkin method is used. The velocity components u and v are expanded in their harmonic constituents M_0 (residual current), M_2 (principal tide), M_4 (first overtide) and so on. In this study the series is truncated after the M_2 components, so nonlinear tides are not accounted for. In *van Leeuwen et al.* (2003) it was shown that at the seaward side of the tidal inlet the dominant transport mechanism was the transport of sediment by the residual currents, while inside the tidal basin higher harmonics of the tide were important. Therefore it is sufficient to calculate the sediment flux by only considering

the M_0 and M_2 components of the velocity field. The validity of this assumption will be discussed in the next chapter. The numerical details of the solution procedure are equal to that described in Chapter 3.

4.4.3 Numerical Method to Solve the Poisson Problem

Each iteration step Equation (4.25) has to be solved for given $\vec{\tilde{q}}_f$. The method employed consists of transforming this Poisson equation into elliptic-cylindrical coordinates. This allows for construction of solutions as multipole series. The results are integral equation for each pole, which are subsequently solved. For more details, see Chapter 3 and *van der Vegt et al.* (2005). In Chapter 3 the symmetric delta was studied. Therefore, it was sufficient to only consider the symmetric poles. Furthermore, the boundary condition that $\partial\tilde{H}/\partial x = 0$ yields that all sine poles are zero. Hence, the bottom pattern is described by the sum of even cosine poles. In this study the bottom patterns can be asymmetric. Therefore the bottom patterns are described by the sum of both odd and even cosine poles.

4.5 Results

The number of collocation points used in this study is $N_x = 40$ for the x-direction and $N_y = 60$ for the y-direction. This is based on several sensitivity experiments and the values have been chosen such that calculations are fast and reasonably accurate. To solve Equation (4.25) every iteration step 150 poles have been used. An overview of the parameter values which are the same for al experiment is given in Table 4.1. The factor γ has been chosen such that $\gamma/\beta = 2$. This factor can be changed, but this will only result in a change of the amplitude of the modeled bottom patterns but does not influence the patterns itself. An overview of the performed experiments and the magnitude of the other parameters is presented in Table 4.2.

The phase of the shore-parallel currents at sea is determined by Equation (4.14). The phase difference between the shore-parallel tidal currents and the cross-shore currents through the tidal inlet is given by $\Phi(0)$. A negative value of $\Phi(0)$ means that the cross-shore currents through the tidal inlet are lagging the shore-parallel tidal currents, which is quite often observed for tidal inlet systems (*Sha and van den Berg*, 1993). A value of $\Phi(0) = 0^\circ$ is representative for tidal inlet systems along the Dutch Wadden Sea, while $\Phi(0) = -90^\circ$ is observed for the Western Scheldt estuary (*Sha and van den Berg*, 1993).

4.5.1 Coriolis force

In the first experiments the influence of the Coriolis force on the asymmetry of the ebb-tidal deltas is studied. The large-scale pressure gradient at sea is zero, $S_0, S_2 = 0$. The only symmetry-breaking mechanism in this experiment is related to the Coriolis force. The Coriolis parameter is $f = 1.11 \cdot 10^{-4}$ s^{-1} for a latitude of 50°. The relative influence of the Coriolis force compared with local acceleration due to inertia is measured by the inverse Rossby number, $Ro^{-1} = fL/U$. Here, L is the typical length scale, which is the width of

Parameter	Value
N_x	40
N_y	60
N_{poles}	150
C_d	$2.5 \cdot 10^{-3}$
A_h	$l * U$ m^{2}s^{-1}
l	14 m
U	Eq. (4.22)
γ	0.7 ms^{-1}
β	0.35

Table 4.1: Parameter values used in the experiments.

section	B (km)	$\hat{U}(0)$ (ms^{-1})	f (s^{-1})	V_2 (ms^{-1})	$\Phi(0)$ (°)	V_0 (ms^{-1})
4.5.1	5	0.3	$1.11 \cdot 10^{-4}$	0	0	0
4.5.2	2	0.5	0	0.15	0	0
4.5.2	2	0.2-0.5	0	0.15	0	0
4.5.2	2	0.5	0	0.025-0.15	0	0
4.5.2	2	0.5	0	0.15	-100-0	0
4.5.2	5 and 7	0.5	0	0.15	0	0
4.5.3	2	0.5	0	0	0	0.01

Table 4.2: Overview of experiments performed for this study.

the inlet. For $\hat{U}(0) = 1$ ms^{-1} and $B = 2$ km the inverse Rossby number is $Ro^{-1} = 0.2$ and its effect is small. To show the influence of the Coriolis force on the asymmetry of the equilibrium bathymetry, results are presented for a relatively broad inlet ($B = 5$ km) with small cross-shore tidal currents ($\hat{U}(0) = 0.3$ ms^{-1}). In this situation $Ro^{-1} = 1.8$ and the influence of Coriolis force is of the same order of magnitude as inertia.

The modeled equilibrium bathymetry is shown in Figure 4.4(a). It is slightly asymmetric with respect to the mid-axis through the tidal inlet. The deepest channel is oriented to the left. The channel on the right-hand side of the inlet is a little shallower than the channel on the left-hand side. There is not a clear channel in the center of the inlet. Most sediment of the delta is located at the right-hand side of the mid-axis through the inlet. The ebb-tidal delta is shifted a little to the right. Figure 4.4(b) shows the residual current pattern. Two residual circulation cells can be recognized as was the case with symmetrical ebb-tidal deltas described in Chapter 3, but they are slightly asymmetric. The residual currents in the right-hand cell are slightly smaller than the currents in the left-hand cell. The ebb-tidal delta is located at the end of the ebb-dominated currents.

Experiments have been performed for smaller inlets and with larger magnitude of $\hat{U}(0)$ (smaller inverse Rossby number). The equilibrium bottom patterns are less asymmetric. For typical configurations as found along the Dutch and German Wadden Sea the influence of the Coriolis is negligible because the inlets have strong magnitudes of the outflow (~ 1 ms^{-1}) and are relatively small (between 2 and 10 km). For tidal inlets which are relatively wide and have relatively small cross-shore tidal currents (inverse Rossby number

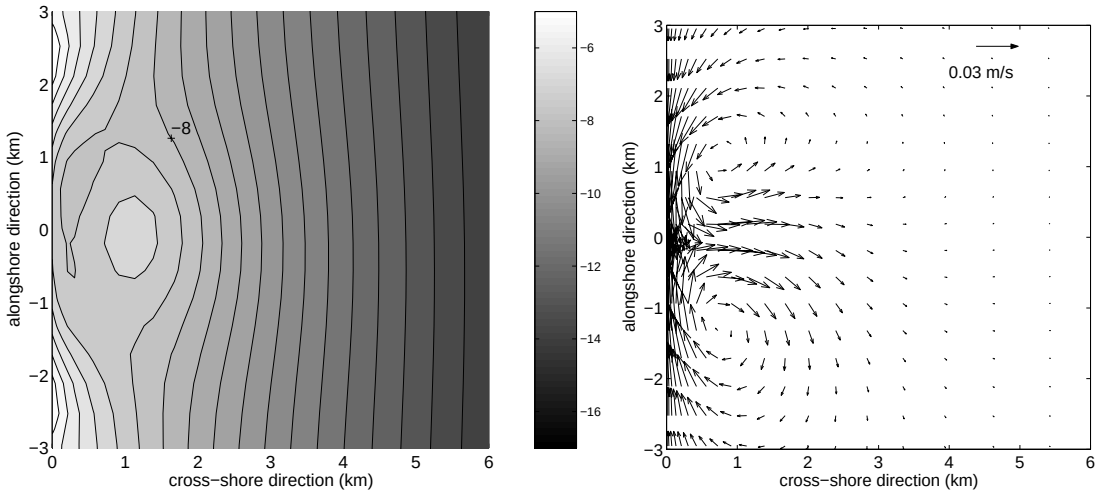

(a) (b)

Figure 4.4: (a) Equilibrium bathymetry for $\hat{U}(0) = 0.3$ ms^{-1}, $B = 5$ km and no large-scale shore-parallel currents. The Coriolis parameter is set for a latitude of 50° north. Contour lines are drawn every 0.5 meter. (b) Residual currents in morphodynamic equilibrium.

is large) the Coriolis force can be important.

On the Southern Hemisphere the Coriolis parameter is negative. In that case the asymmetry changes from right-oriented to left-oriented.

4.5.2 Shore-parallel currents

In this subsection the influence of the interaction between the shore-parallel and cross-shore tidal currents on the (a)symmetry properties of ebb-tidal deltas is studied. It is assumed that the deltas are located at the Northern Hemisphere. Similar results for the Southern Hemisphere can be obtained by increasing $\Phi(0)$ with 180°.

Default case

In the first series of experiments the width of the inlet is $B = 2$ km. The maximum tidal currents at $x = 0$ induced by the alongshore pressure gradient in the reference state is $V_2(0) = 0.15$ ms^{-1}. The magnitude of $\hat{U}(0)$ is varied between $\hat{U}(0) = 0$ and $\hat{U}(0) = 0.5$ ms^{-1}. For increasing magnitude of $\hat{U}(0)$ also the typical velocity scale U increases (see Equation (4.22)). Therefore, also the magnitude of the friction coefficient r and the magnitude of the diffusion parameter A_h increase. As a consequence, for increasing magnitudes of the outflow in principle both the reference state velocity profile and phase would change (Equations (4.14)). However, in the experiments presented in this section it is chosen to study the influence of a change in $\hat{U}(0)$ while keeping the phase Φ and the magnitude V_2 of the reference state velocity fixed. This profile is calculated with a friction parameter $r = (8/3\pi)C_d V_2(0)$. The pressure gradient is such that $V_2(0) = 0.15$

ms^{-1}. To calculate $\tilde{u}$ and $\tilde{v}$ it is used that $r = 8/3\pi C_d U$, and U is given by Equation (4.22).

The residual currents in morphodynamic equilibrium for $\hat{U}(0) = 0.5$ ms^{-1} are shown in Figure 4.5(a). Two cells are present, with the residual currents in the right-hand cell being larger than those in the left-hand cell. Figure 4.5(b) shows the tidal ellipses of the M_2 tidal currents. From this figure it is concluded that the M_2 tidal currents are large and bidirectional at the left-hand side of the inlet and weak and more rotary at the right-hand side. Furthermore, the area with ebb-dominated currents is located at the left-hand side of the mid-axis through the tidal inlet. A vector plot of the residual sediment transport $\vec{q}_{\mathrm{f}}$ is shown in Figure 4.5(c). Sediment is transported from the right-hand side of the inlet to the center of the inlet. From there it is transported seaward to the left-hand side of the inlet. The equilibrium bathymetry is shown in Figure 4.5(d). Most sediment of the ebb-tidal delta is positioned at the left-hand side. There is not a clear isolated ebb-shoal (no closed contour lines) as was obtained in the case of the symmetric deltas (Chapter 3) or in the experiment with Coriolis force (previous section). Instead, the delta starts at the left-hand side of the inlet and protrudes seaward until approximately $x = 1$ km and $y = 0$. The main channel is oriented to the right. It has a maximum depth of 8 meter and has flood-dominant currents. Although the currents are strong, bidirectional and ebb-dominated at the left-hand side of the inlet, there is no clear channel in that area. The strong bidirectional tidal currents at the left-hand side of the inlet transport sediment, but this sediment transport is convergent and is balanced by the convergence of the bed-slope induced sediment transport. This results in the presence of an ebb-tidal delta without a clear ebb-dominated channel.

It has been studied whether the profile of V_2 has a strong influence on the results. In the calculation of V_2 it was used that the friction coefficient was $r = (8/3\pi)C_d V_2(0)$ and $V_2(0) = 0.15$ ms^{-1}. An experiment has been performed in which V_2 was calculated with a friction coefficient $r = 8/3\pi C_d U$, and U as given by Equation (4.22). From the results it is concluded that it has only a small influence on the final equilibrium (Figure 4.6).

Sensitivity of the results to magnitude of the tidal currents through the inlet

To obtain the results described in the previous section, the magnitude of $\hat{U}(0)$ was increased with steps of 0.1 ms^{-1}. To quantify the "amount of asymmetry", an objective parameter is introduced. Because the maximum of the shoal or the minimum of the channel does not exist in all experiments that have been performed, the alongshore position of the maximum of $\tilde{H}$ is used as a measure for the asymmetry of the ebb-tidal delta. This parameter is called y_p. When y_p has a negative value, most sediment is on the right-hand side of the inlet. The ebb-delta is always located seaward of the area where currents are ebb-dominated. This implies that when most sediment is located at the right-hand side of the inlet, also the area with ebb-dominated currents is located at the right-hand side. Hence, the delta is called right-oriented. A positive value of y_p implies that the delta is left-oriented.

In Figure 4.7(a) y_p is shown as a function of $\hat{U}(0)$. For $\hat{U}(0) = 0.2$ ms^{-1} the delta is right-oriented. For larger values the delta is left-oriented. Increasing $\hat{U}(0)$ results in an increase of y_p. The increase in y_p becomes smaller for larger values of $\hat{U}(0)$.

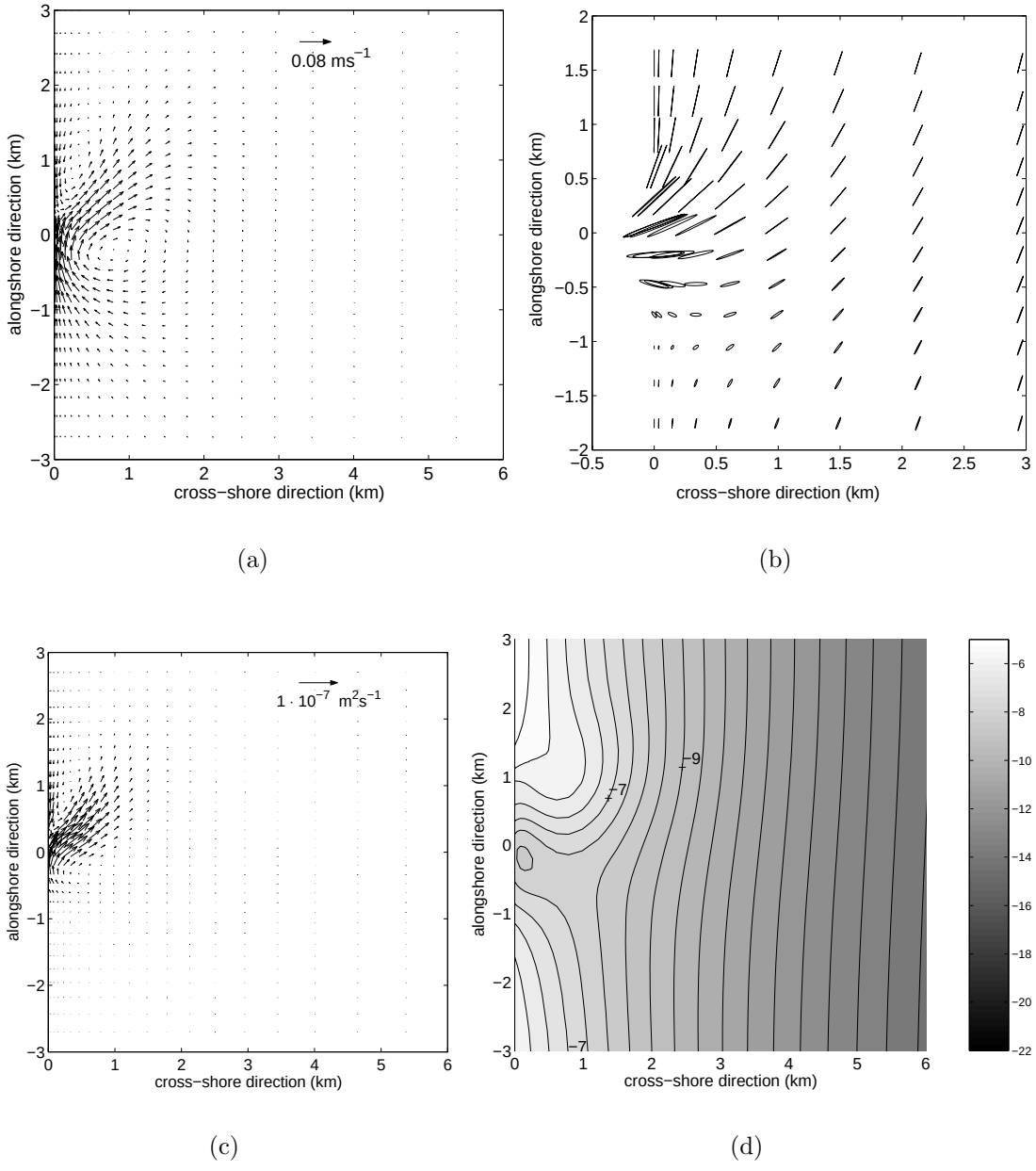

Figure 4.5: (a) Residual currents for $\hat{U}(0) = 0.5$ ms^{-1}, $V_2(0) = 0.15$ ms^{-1}, $\Phi(0) = 0^\circ$, $f = 0$ and $B = 2$ km. (b) Same as (a), but now the current ellipses of the M_2 tide. (c) Same as (a), but now residual sediment transport in morphodynamic equilibrium is shown for $\alpha = 10^{-5}$ s^{2}m^{-1}. (d) Same as (a), but now the equilibrium bathymetry is shown. Contour lines are drawn every 0.5 meter.

Sensitivity of the results to magnitude of the shore-parallel tidal currents

In the experiments described in this subsection $\hat{U}(0) = 0.5$ ms^{-1}, $\Phi(0) = 0^\circ$ and $V_2(0)$ is increased from zero to 0.15 ms^{-1}. The reference velocity profile is calculated as in the previous sections. This means that V_2 and Φ are calculated with $r = (8/3\pi)C_d V_2(0)$. For the

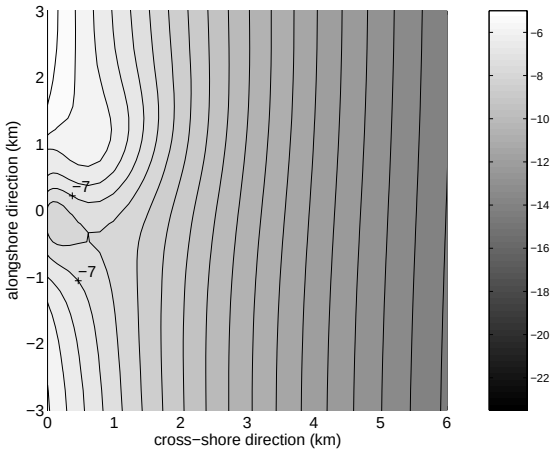

Figure 4.6: Same as Figure 4.5(d), but now V_2 has been determined with $r = 8C_dU/(3\pi)$, so U given by Equation (4.22) instead of $U = V_2(0)$.

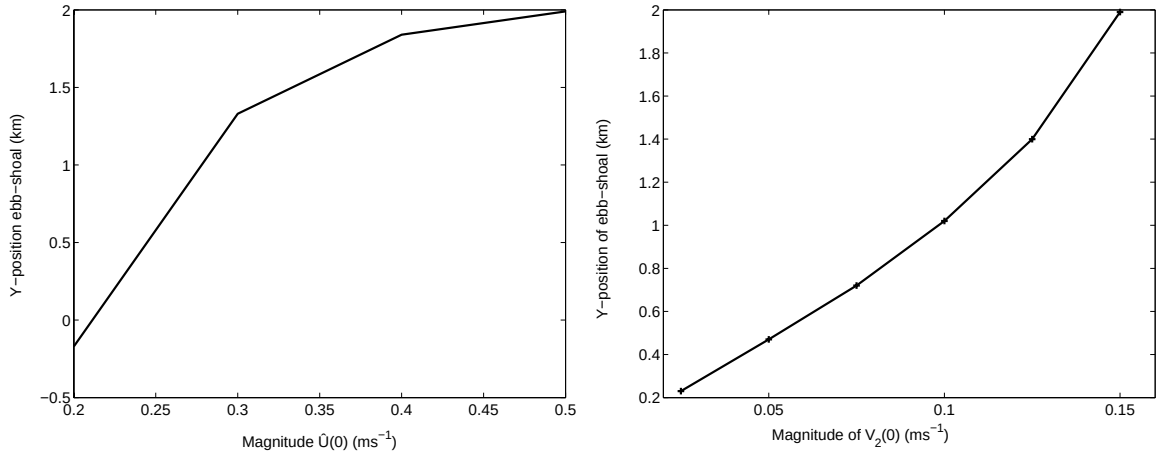

(a) (b)

Figure 4.7: (a) The y-coordinate of the position of the ebb-shoal for $B = 2$ km, $V_2(0) = 0.15$ ms^{-1}, $\Phi(0) = 0°$ and $f = 0$ as a function of $\hat{U}(0)$. (b) The y-coordinate of the position of the ebb-shoal for $B = 2$ km, $\hat{U}(0) = 0.5$ ms^{-1}, $\Phi(0) = 0°$ and $f = 0$ as a function of $V_2(0)$.

calculations of $\tilde{u}$ and $\tilde{v}$ it is used that $r = 8/3\pi)C_dU$, with U as given in Equation (4.22).

Again, the value of y_p has been determined for each experiment. In this parameter setting for each value of $V_2(0)$ the value of y_p is positive. This means that the area with ebb-dominated currents and the area where most sediment of the ebb-tidal delta is located, is found on the left-hand side of the tidal inlet. Increasing the magnitude of $V_2(0)$ causes a faster than linear increase of y_p (Figure 4.7(b)).

Sensitivity of the results to $\Phi(0)$

According to *Sha and van den Berg* (1993), the phase difference between the cross-shore and shore-parallel currents is an important factor for the asymmetry properties of ebb-tidal deltas. Therefore, in the next experiment the sensitivity of the results to the phase $\Phi(0)$ is studied. The width of the inlet is $B = 2$ km, $\hat{U}(0) = 0.5$ ms^{-1} and $V_2(0) = 0.15$ ms^{-1}. The phase is changed from $\Phi(0) = -100^\circ$ to $\Phi(0) = 0^\circ$.

A vector plot of the residual currents for $\Phi(0) = -100^\circ$ is shown in Figure 4.8(a). The residual currents are organized in two cells and magnitudes of the currents in the two cells are of the same order. Compared to the case that $\Phi(0) = 0^\circ$ (Figure 4.5(a)), the magnitudes of the residual currents are smaller and the two cells are less asymmetric. Furthermore, the area with ebb-dominated currents is now found on the right-hand side of the inlet. The tidal current ellipses of the M_2 tide are strongly polarized on both sides of the tidal inlet (Figure 4.8(b)). The residual sediment transport $\vec{q}_f$ is shown in Figure 4.8(c) and is organized in two cells. Compared to the case that $\Phi(0) = 0^\circ$, the sediment is transported less far seaward and it is transported to the right-hand side of the inlet instead of being transported to the left-hand side. Figure 4.8(d) shows the equilibrium bottom pattern. The flood-dominated channel is oriented to the left and most sediment is found on the right-hand side of the tidal inlet. The delta has now become right-oriented. The bottom pattern is less pronounced than that obtained for $\Phi(0) = 0^\circ$.

The equilibrium bathymetry has been calculated for $\Phi(0) = -100^\circ, -75^\circ, -50^\circ, -25^\circ$ and for $\Phi(0) = 0^\circ$. The value of y_p as a function of $\Phi(0)$ is shown in Figure 4.9. For $B = 2$ km y_p is positive for most values of $\Phi(0)$. However, for $\Phi(0) \approx -80^\circ$ the delta changes orientation. In that case the area with ebb-dominated currents and the area where most sediment of the ebb-tidal delta is found is located at the right-hand side.

Sensitivity of the results to width of the tidal inlet

The width of the inlets along the Dutch coast ranges between approximately two kilometers and ten kilometers. Therefore, in the following experiment the width of the inlet has been varied between these extremes. The flow profile was not changed. This is done to facilitate the comparison between the results, although it is realized that the prescribed velocity profile (4.21) is a reasonable approximation for relatively small inlets (up to 1-2 kilometers), but it is not very realistic for an inlet with $B = 10$ km.

The parameters used in the experiments are $\hat{U}(0) = 0.5$ ms^{-1}, $V_2(0) = 0.15$ ms^{-1} and $\Phi(0) = 0$. The equilibrium bathymetry for $B = 2$ km was already presented in Figure 4.5(d). The equilibrium bathymetry for B =5 km and $B = 7$ km are shown in Figure 4.10(a) and 4.10(b), respectively. For $B = 10$ km no equilibrium bathymetry was obtained for this setting. Interestingly, for $B = 7$ km a second channel appears on the left-hand side. This channel is not present for $B = 2$ km and has approximately the same depth as the channel on the right-hand side. The currents in this channel are flood-dominated. The presence of the channel on the left-hand side is already noticeable in the equilibrium bathymetry for $B = 5$ km. For both $B = 5$ km and $B = 7$ km the area with ebb-dominated currents is found on the left-hand side. Increasing the width of the tidal inlet causes a change in the asymmetry properties. This is also confirmed by the results

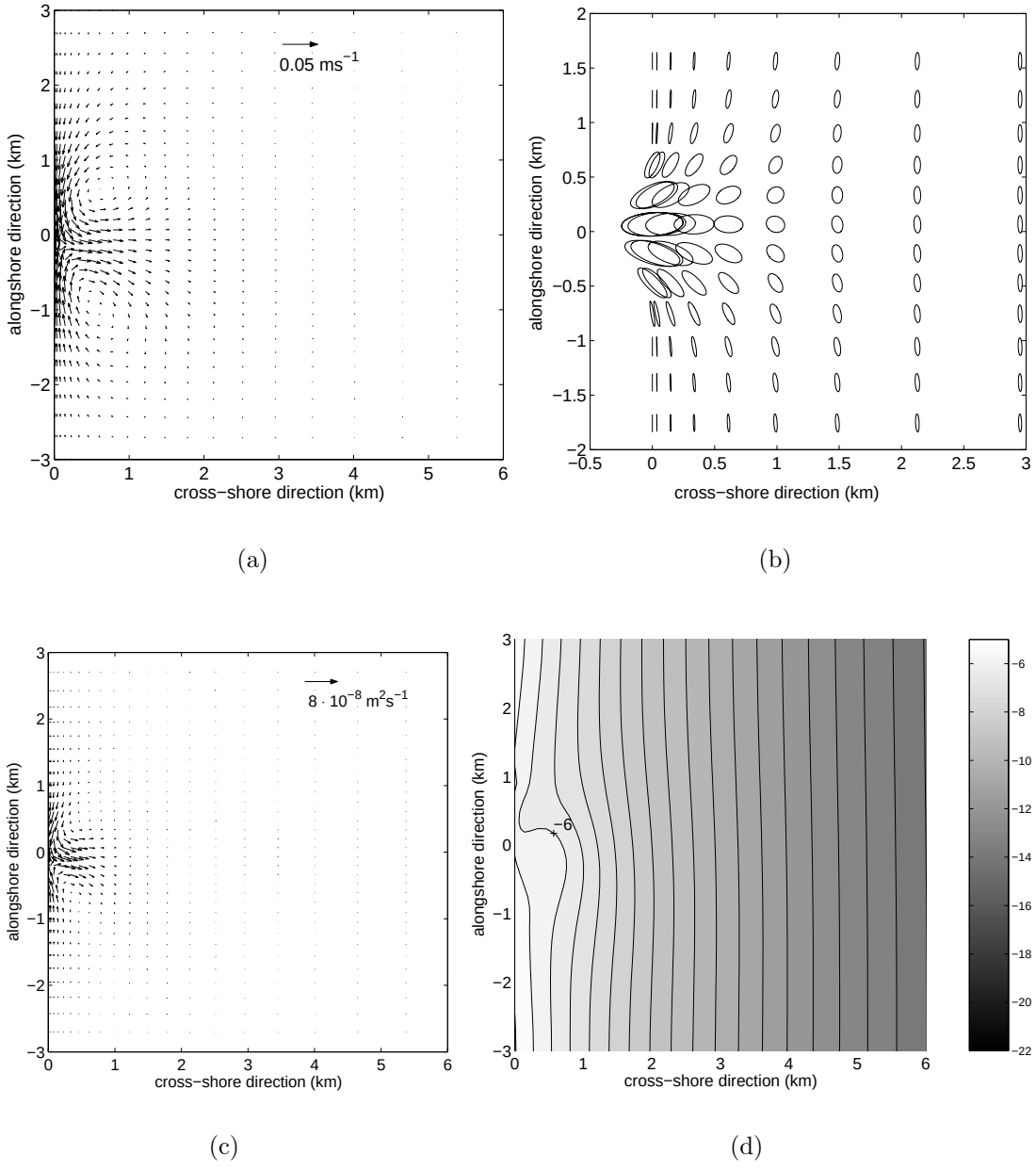

Figure 4.8: As Figure 4.5, except that in this experiment $\Phi(0) = -100°$.

presented in Figure 4.9. The solid line shows y_p as a function of $\Phi(0)$ for $B = 7$ km, $V_2 = 0.15$ ms^{-1} and $\hat{U}(0) = 0.5$ ms^{-1}. While for $B = 2$ km the delta changes orientation for $\Phi(0) \approx -80°$, for $B = 7$ km the delta changes orientation for $\Phi(0) \approx -60°$.

4.5.3 Residual currents at sea

In this section the influence of a prescribed residual shore-parallel current on the asymmetry of the ebb-tidal delta is studied. The width is $B = 2$ km, the Coriolis force is absent,

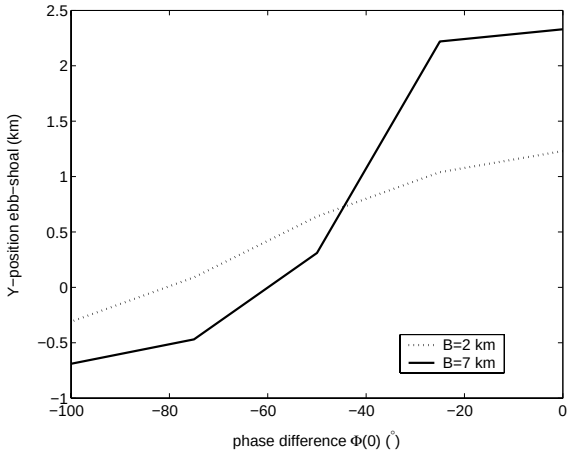

Figure 4.9: The y-coordinate of the position of the ebb-shoal for $\hat{U}(0) = 0.5$ ms^{-1}, $V_2(0) = 0.15$ ms^{-1}, $f = 0$ and $B = 2$ km and $B = 7$ km as a function of the phase difference $\Phi(0)$ between alongshore tidal currents and currents through the tidal inlet.

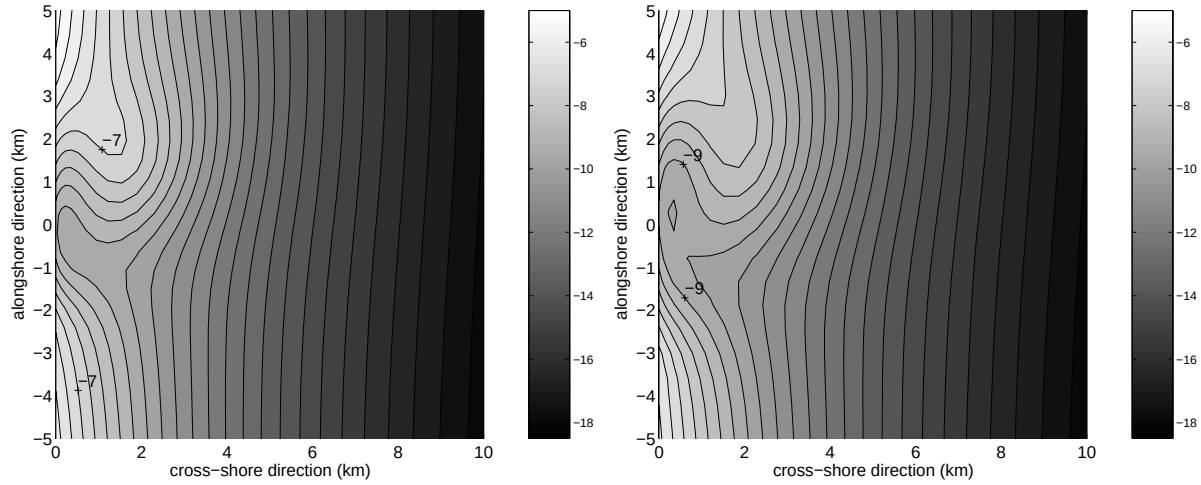

(a) (b)

Figure 4.10: (a) Equilibrium bathymetry for $\hat{U}(0) = 0.5$ ms^{-1}, $V_2(0) = 0.15$ ms^{-1}, $\Phi(0) = 0°$, $f = 0$ and $B = 5$ km. Contour lines are drawn every 0.5 meter. (b) Same as (a), but now for $B = 7$ km.

$\hat{U}(0) = 0.5$ ms^{-1} and the large-scale alongshore current only has a mean component, $S_2 = 0$ and $S_0 \neq 0$. A value for S_0 is chosen such that $V_0(0)$ = -0.01 ms^{-1} and for $x \to \infty$ V_0 is -0.05 ms^{-1}. The residual currents are in the negative y-direction. In Figure 4.11(a) the equilibrium bathymetry is shown. The ebb-tidal delta is located at the right-hand side of the tidal inlet. The deepest channel is oriented against the direction of the residual currents. A vector plot of the residual currents is shown in Figure 4.11(b). The residual circulation pattern is also asymmetric. Changing the direction of the large-scale residual currents changes the orientation of the delta.

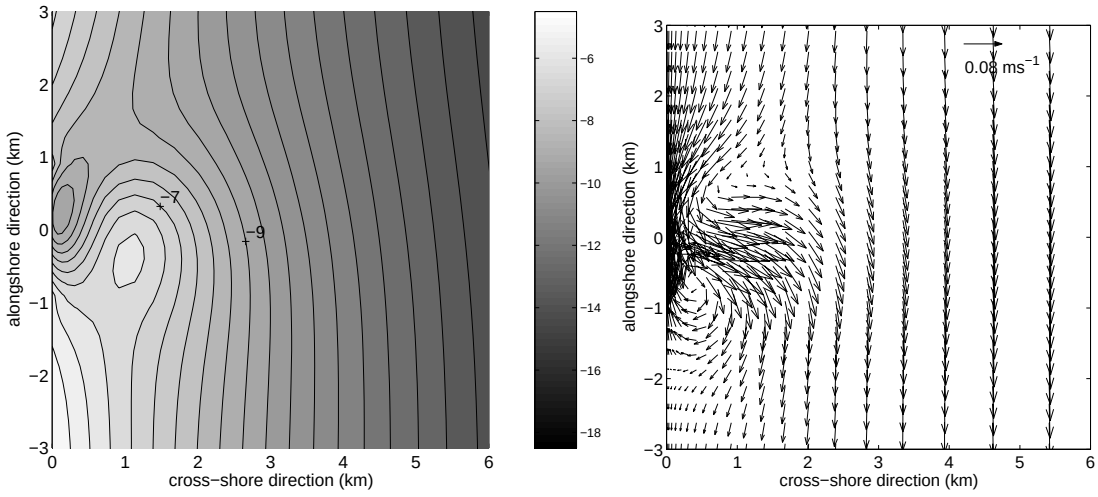

(a) (b)

Figure 4.11: (a) Equilibrium bathymetry for large-scale alongshore mean current from left to right. $\hat{U}(0) = 0.5$ ms^{-1}, $V_0(0) = -0.01$ ms^{-1} , $f = 0$ and $B = 2$ km. Contour lines are drawn every 0.5 meter. (b) Mean currents in morphodynamic equilibrium.

In a last experiment the influence of both residual and tidal shore-parallel tidal currents is studied. The Ameland Inlet (see figure 1.7) is characterized by residual currents which are directed in the negative y-direction and by shore-parallel tidal currents with a small phase difference $\Phi(0)$ (*Ridderinkhof*, 1989; *Sha*, 1989a; *Israel and Dunsbergen*, 1999). The effects of the residual currents and the shore-parallel tidal currents are counteracting, as they cause the delta to become right-oriented and left-oriented respectively. In the following experiment $B = 2$ km, $\hat{U}(0) = 0.5$ ms^{-1}, $V_2(0) = 0.15$ ms^{-1}, $\Phi(0) = 0^\circ$ and the magnitude of $V_0(0)$ is gradually increased from -0.01 ms^{-1} to -0.03 ms^{-1}. The equilibrium bathymetry for $V_0(0) = -0.01$ ms^{-1} is shown in Figure 4.12(a) and for $V_0(0) = -0.03$ ms^{-1} it is shown in Figure 4.12(b). For $V_0(0) = -0.01$ ms^{-1} the delta is left-oriented, while for $V_0(0) = -0.03$ ms^{-1} the delta is right-oriented. In both cases the main channel is flood-dominated and the ebb-tidal delta is found at the seaward end of the area with ebb-dominated currents.

4.6 Discussion and conclusions

The main aim of this study was to investigate the influence of several tide-related processes on the (a)symmetry properties of ebb-tidal deltas. If the area with ebb-dominated currents is located at the left-hand side of the tidal inlet the delta is called left-oriented, if the area with ebb-dominated currents is located at the right-hand side the delta is called right-oriented. In this section both the modeled hydrodynamics and the modeled bottom pattern are discussed and compared with both field observations and with results of previous studies. The several processes that were included in the model and that lead to

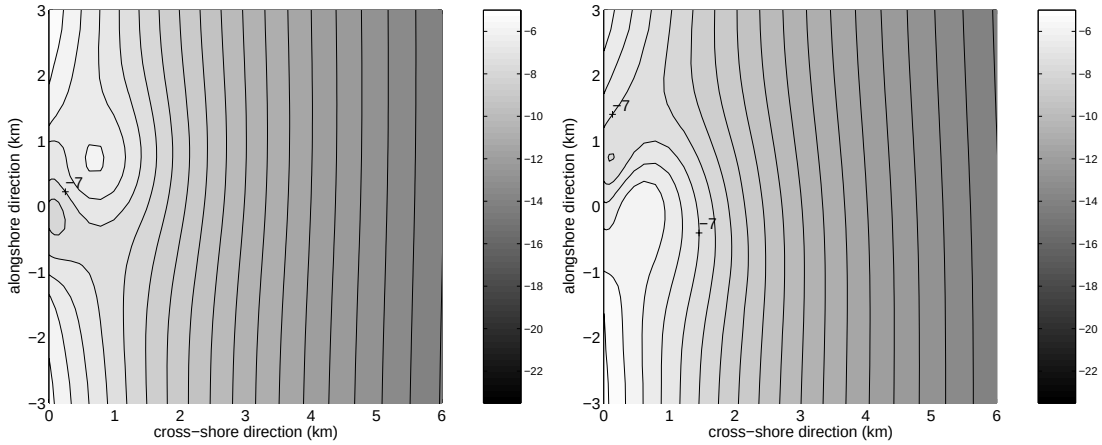

(a) (b)

Figure 4.12: (a) Equilibrium bathymetry for $B = 2$ km, $\hat{U}(0) = 0.5$ ms^{-1}, $V_2(0) = 0.15$ ms^{-1}, $\Phi(0) = 0°$, $f = 0$ and $V_0(0) = -0.01$ ms^{-1}. Contour lines are drawn every 0.5 meter. (b) Same as (a), but now $V_0(0) = -0.03$ ms^{-1}.

asymmetric ebb-tidal deltas are subsequently discussed. A brief physical interpretation of the results obtained is presented. This section ends with suggestion for further research.

4.6.1 Coriolis force

The influence of the Coriolis force on the asymmetry of the ebb-tidal delta is only small. Only for wide inlets with small magnitudes of the cross-shore tidal currents its influence becomes noticeable. In these situations delta is right-oriented. However, it is hard to compare these results with existing studies or with observed asymmetric ebb-tidal deltas. The effect is too small to be measured and other processes turn out to be more important for the asymmetry of ebb-tidal deltas.

The mechanisms that lead to asymmetry of the ebb-tidal delta can be explained by vorticity concepts (*Zimmerman*, 1981). Because the delta is always found at the seaward end of the area where currents are ebb-dominated, the main clue is to explain the mechanisms that cause the asymmetry in the two residual circulation cells. In the symmetric case the transfer of tidal vorticity (generated by the shear in the prescribed velocity profile over the inlet) by the tidal currents is such that positive residual vorticity is generated at the left-hand side of the tidal inlet and negative residual vorticity at the right-hand side (for a detailed discussion, see Chapter 3).

The torque induced by the Coriolis force is an additional source of tidal vorticity. During ebb the tidal currents transport the planetary vorticity seaward. Because the water depth is increasing, positive tidal vorticity is generated due to vortex stretching. This additional tidal vorticity enhances the magnitude of the tidal vorticity at the left-hand side (where the vorticity becomes more positive) and reduces the magnitude at the right-hand side of the mid-axis of the inlet (where the vorticity becomes less negative).

This vorticity is transferred by the tidal currents. Because this transport is convergent, large positive residual vorticity is generated at the left-hand side (the area $x > 0$ and $y > 0$)and small negative residual vorticity at the right-hand side of the inlet (the area $x > 0$ and $y < 0$). During flood the vortex stretching related to the planetary vorticity transport enhances the magnitude of the vorticity at the left-hand side (where the vorticity becomes more negative) and diminishes the magnitude at the right-hand side of the mid-axis of the inlet (where the vorticity becomes less positive). Hence, the vorticity fluxes have the same sign and magnitude as during ebb and therefore also during flood large positive residual vorticity is generated at the left-hand side and small negative residual vorticity at the right-hand side of the inlet. As a consequence, there is large positive mean vorticity at the left-hand side and small negative mean vorticity at the right-hand side of the inlet. This results in the residual circulation cells as modeled in Section 4.5.1.

4.6.2 Shore-parallel tidal currents

In the experiment described in Section 4.5.2 the width of the inlet is 2 km, $\hat{U}(0) = 0.5$ ms^{-1}, $f = 0\ \mathrm{s}^{-1}$, $V_2(0) = 0.15\ \mathrm{ms}^{-1}$ and $\Phi(0) = 0°$. The modeled tidal currents on the left-hand side of the tidal inlet are strong and bidirectional, while on the right-hand side they are weaker and more rotary. The modeled residual currents results in an area with ebb-dominated currents which is located at the left-hand side of the mid-axis through the inlet. At the right-hand side the currents are flood-dominated. These modeled hydrodynamics are in agreement with observations in the Texel Inlet (*Sha*, 1989b). Furthermore, they are consistent with the conceptual model of *Sha* (1989a). The model results are also consistent with the modeled hydrodynamics of the Ameland Inlet by *Ridderinkhof* (1989). The residual circulation patterns are quite similar.

The model results of Section 4.5.2 show that the sediment is transported seaward from the center of the inlet to the left-hand side. At the right-hand side of the inlet the sediment is transported from the sea to the inlet. This mean sediment transport $\vec{\bar{q}}_{\mathrm{f}}$ is in gross agreement with observed sediment transport patterns in the Texel Inlet (*Sha*, 1989b).

The model results show that the seaward transport of sediment at the left-hand side of the inlet is convergent and causes the presence of an ebb-tidal delta. No ebb-dominated channel is modeled. On the right-hand side of the mid-axis thought the inlet a flood-dominated channel is modeled. This modeled bottom pattern is consistent with those obtained in Chapter 3 and 5. There it was also found that the ebb-tidal delta is located in the area where the strength of the ebb-dominated currents is decreasing. Furthermore, the model results are consistent with the findings of *Schuttelaars et al.* (2003). They performed experiments that represent the hydrodynamic setting of the Dutch Wadden Sea by modeling a traveling wave along the coast. This coast was interrupted by a tidal inlet. They took into account the dynamic interaction between the backbarrier basin and the sea and used a local formulation of the sediment transport (the formulation of *Engelund and Hansen* (1967)). The modeled initial erosion-deposition rates showed that the channel was oriented in the direction of propagation of the tidal wave, that is to the right in the convention adopted in this study. The delta was found on the left.

Although the modeled bottom patterns are consistent with previous studies, they are

not in complete agreement with observed bottom patterns of ebb-tidal deltas along the Dutch Wadden Sea. The model results predict that most sediment of the delta is located at the left-hand side. This is in gross agreement with the predictions of *Sha* (1989a), which is based on observations of the ebb-tidal deltas of the Dutch Wadden Sea. However, the model predicts the presence of a channel on the right-hand side of the mid-axis through the inlet. This deep channel is not found in observations. Furthermore, no ebb-dominated channel is modeled. Observations show the presence of deep ebb-dominated channels which are oriented to the left. In addition, the observations suggest the presence of an almost shore-parallel flood-dominated current at the left-hand side. This is not recovered with the model.

The model results are sensitive to several parameters. However, the delta is always located at the seaward end of the area with ebb-dominated currents. The modeled channel has flood-dominated currents and is always located at the opposite side of where the ebb-tidal delta is found. The results show that increasing the magnitude of $V_2(0)$ while keeping the other parameters constant, results in an increase of the asymmetry of the ebb-tidal delta. Increasing the magnitude of $\hat{U}(0)$ while keeping other parameters constant, also results in an increase of the asymmetry of the delta. Furthermore, when the tidal currents in the inlet are significantly lagging the shore-parallel tidal currents at sea, the delta can change orientation. For $B = 2$ km this occurs for $\Phi(0) \approx -80°$, while for $B = 7$ km this occurs for $\Phi(0) \approx -60°$. Hence, increasing the width of the inlet causes the delta to be less asymmetric.

The residual circulation patterns obtained with the model can again be understood by analyzing the vorticity balance. However, this analysis is quite elaborate and is therefore not presented in detail. In Chapter 2 the growth or decay of coastline perturbations was determined by the relative strength of the alongshore gradient of the vorticity fluxes in the alongshore direction and the cross-shore gradient of the vorticity fluxes in the cross-shore direction. An analysis revealed that for the locations of the centers of the residual circulation cells with respect to the mid-axis through the inlet a similar competition is important. The locations and magnitudes of these residual circulation cells determine the area where the currents are ebb-dominated. The total mean vorticity flux partly involves terms that describe the transfer of vorticity generated at the tidal inlet ($\tilde{\omega}$) by the velocity components $\tilde{u}$ and $\tilde{v}$. This is the vorticity flux that causes the two residual circulation cells in the symmetric case (see Chapter 3). The other part of the mean vorticity flux is due to the joint presence of externally forced shore-parallel tidal currents and the tidal currents which are due to the presence of the tidal inlet. The tidal velocity components $\tilde{u}$ and $\tilde{v}$ transfer the vorticity of the reference state Ω and the shore-parallel tidal currents V transfer the vorticity due to the presence of the inlet $\tilde{\omega}$. The alongshore gradient of this 'interaction' vorticity flux in the alongshore direction ($\partial/\partial y[V\tilde{\omega} + \tilde{v}\Omega]$) results in residual circulation cells that cause the area with ebb-dominated currents to be located at the left-hand side, while the cross-shore gradient of the vorticity fluxes in the cross-shore direction ($\partial/\partial x[\tilde{u}\Omega]$) results in residual circulation cells that cause the area with ebb-dominated currents to be located at the right-hand side of the mid-axis through the inlet. In most cases the alongshore convergence is dominant and the area with ebb-dominated currents is located at the left-hand side. For broader inlets the convergence of the cross-shore 'interaction' vorticity flux can be dominant and the orientation of the delta changes.

4.6.3 Residual currents at sea

In Section 4.5.3 the influence of residual currents at sea was studied. These currents are caused by a large-scale residual pressure gradient along the Dutch coast. In the case that these currents are in the negative y-direction, the area with ebb-dominated currents is located at the right-hand side of the mid-axis through the inlet. Also the sediment is transported seaward from the center of the inlet to the right. The modeled ebb-tidal delta is located at the right. No ebb-dominated channel is modeled. The modeled channel is located at the left-hand side of the inlet and has flood-dominated currents.

It is hard to compare the results with observations. Most observations concern the case that the residual currents at sea are forced by the waves. These wave-driven currents are very strong and confined to a small area near the coast. The currents modeled in this study are driven by the tide. However, the model results are consistent with the findings of *Schuttelaars et al.* (2003). They also found that the delta is located at the right-hand side of the inlet when the mean currents at sea are from left to right.

The asymmetry of the flow and bottom pattern caused by the large-scale mean flow is mainly due to the superposition of the currents induced by the dipole of the symmetric case and the currents induced by the large-scale mean flow (Figure 4.13). This causes a dipole which is asymmetric. The circulation cell at the left-hand side is enhanced. The right-hand circulation cell is weakened. The mean sediment transport is such that sediment is removed from the tidal inlet and is transported offshore to the right-hand side of the inlet. This causes a delta at the right-hand side and the ebb-tidal delta is right-oriented.

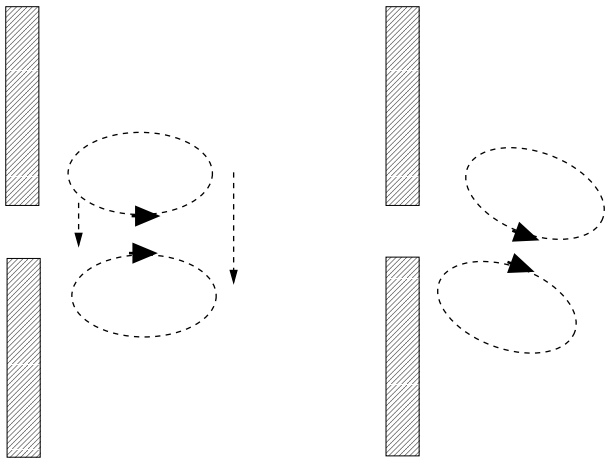

Figure 4.13: Influence of adding a large scale residual flow to a situation when two residual circulation cells are present (as calculated in the symmetric case). Two residual circulation cells are represented by the two dashed ellipses. Large scale mean current is represented by dashed arrow. Adding these two residual currents results in an asymmetric residual current pattern as shown in the right panel.

4.6.4 Suggestions for further research

The modeled hydrodynamics seem to be consistent with field data. However, the modeled bottom patterns do not agree with observations. We will discuss possible reasons that cause the discrepancy between modeled bottom patterns and observed ones. This also motivates the suggestions for further research.

First, in the idealized model no backbarrier basin is present. The prescribed velocity profile over the inlet is fixed and does not follow from physical laws. In reality the velocity profile will change when the depth in the inlet changes. When it becomes deeper the effect of friction decreases and the velocity will increase. Furthermore, in contrast to the backbarrier basins observed along the east US-coast (Georgia, South Carolina), the backbarrier basins of the Dutch Wadden Sea are very shallow. In shallow water the tide has a traveling wave character. In a traveling wave, water is transported in the direction of the wave, the so-called Stokes drift. In *van Leeuwen et al.* (2003) the Frisian Inlet was modeled. They took into account the backbarrier basin. This basin was shallow (uniform depth of 2 m). Their results suggest the importance of Stokes drift in the generation of the ebb-tidal delta. Because equilibrium was never reached, their results can not be used to determine whether Stokes drift is also important for the maintenance of the asymmetric ebb-tidal delta. Furthermore, the results of *Schuttelaars et al.* (2003) suggest that Stokes drift is not important for the dynamics of asymmetric ebb-tidal deltas. However, it should be noted that their backbarrier basin was relatively deep (10 m) and is therefore more representative for a backbarrier basin observed along the east US-coast. It is expected that for such deep backbarrier basin Stokes drift is not important. In the idealized model Stokes drift is not modeled because the rigid lid approximation was applied. Therefore, to study the possible influence of such a Stokes drift a relatively shallow backbarrier basin should be added to the model geometry. Furthermore, no rigid lid approximation should be used. In view of many other simplifying assumptions in the hydrodynamics (e.g., the linearized bed shear-stress formulation), it would be very interesting to use a state-of-the-art morphodynamic model (like Delft3D) and to adapt it such that morphodynamic equilibria can be calculated.

Second, the sediment transport only includes effects of tidal currents and has a local character. No time-lag effects were taken into account. To study such an effect, a suspended-load sediment transport formulation should be used instead of a bedload sediment transport formulation. Previous studies suggest that this may be important. *Murray* (2004) showed that neglecting such effects prevented the formation of channels in his morphodynamic model of the nearshore zone. Furthermore, no effects of waves or wind were accounted for in this study. Observations show that wave influence is considerable for the Dutch Wadden Sea *Sha* (1989a). In addition, the effect of a critical velocity for erosion was not taken into account. For coarse sediment this critical velocity for erosion might be up to 0.3 ms^{-1}.

Third, no 3D effects have been modeled with the idealized model. In the case that the channels are bending, curvature effects may become very important.

The last aspect that should be mentioned here is that U was taken as a constant. However, the magnitude of the tidal currents changes one order of magnitude in the region of the tidal inlet. This also implies that U should change one order of magnitude

and calculations should be performed with a spatially dependent U. Hence, the friction coefficient r will become spatially dependent. This might influence the asymmetry of the residual circulation cells. Furthermore, $\vec{\tilde{q}}_{\mathrm{bot}}$ will also vary due to spatial variations in U instead of variations in $\vec{\nabla}\tilde{H}$ only.